ORIGINAL ARTICLE
Iran J Allergy Asthma Immunol
In press.

Silencing *LIMK1* Can Inhibit ROS-mediated NF-κB/NLRP3 Pathway Activation and Reduce Inflammatory Injury in H9c2 Cardiomyocytes

Zhijian Huang, Youxiao Zeng, Xue'e Huang, Lihong Huang, Yafen He, and Yijun Zhou

Department of Geriatrics, Quanzhou First Hospital Affiliated to Fujian Medical University, Quanzhou, Fujian, China

Received: 10 November 2025; Received in revised form: 26 March 2026; Accepted: 9 May 2026

ABSTRACT

Heart failure (HF) represents the final stage of multiple cardiovascular disorders. Although LIMK1 regulates cytoskeletal dynamics and contributes to cardiac fibrosis, its exact role in HF remains uncertain.

To establish an in vitro HF model, H9c2 cells were treated with isoproterenol (ISO), and LIMK1 expression was analyzed. LIMK1 was silenced using small interfering RNA to investigate its role in cell injury, hypertrophy, fibrosis, cytoskeletal dynamics, and apoptosis. Oxidative stress, reactive oxygen species (ROS), 8-hydroxy-2'-deoxyguanosine (8-OHdG), MDA, SOD, GSH-Px, NADPH oxidase, inflammation, and mitochondrial function were also assessed. Furthermore, the interplay between LIMK1, ROS, and nuclear factor kappa-light-chain-enhancer of activated B cells (NF-κB)/NOD-like receptor family pyrin domain containing 3 (NLRP3) signaling was explored using hydrogen peroxide (H2O2; a ROS inducer), diprovocim (an NF-κB activator), and N-acetylcysteine (NAC; a ROS inhibitor).

ISO treatment significantly upregulated the expression of LIMK1 in H9c2 cells. Silencing LIMK1 alleviated ISO-induced myocardial cell damage, hypertrophy, and fibrosis, inhibited Cofilin phosphorylation and F-actin expression, and reduced cell apoptosis and ROS production, thereby mitigating oxidative damage. Furthermore, LIMK1 silencing reduced mitochondrial ROS levels, restored mitochondrial membrane potential, and inhibited the release of inflammatory cytokines. However, H2O2 partially reversed the protective effect of LIMK1 silencing. LIMK1 silencing alleviated inflammatory injury by inhibiting NF-κB phosphorylation and NLRP3 expression, and these effects were partially reversed by an NF-κB activator. NAC alleviated cell damage by inhibiting ROS, and its protective effect was also partially reversed by the NF-κB activator.

In conclusion, silencing LIMK1 can suppress ROS-mediated activation of the NF-κB/NLRP3 pathway, thereby alleviating cardiomyocyte injury and the inflammatory response.

Keywords: Heart failure; Inflammation; LIM domain kinase 1; Nuclear factor-kappa B; NLRP3 inflammasome; Reactive oxygen species

Corresponding Author: Yijun Zhou, MD;
Department of Geriatrics, Quanzhou First Hospital Affiliated to Fujian Medical University, Quanzhou, Fujian, China. Tel: (+86 159) 8002 8877, Email: zhou71072025zs@hotmail.com

INTRODUCTION

Heart failure (HF), as the final pathological outcome of multiple cardiovascular disorders, is principally

Published by Tehran University of Medical Sciences (http://ijaai.tums.ac.ir)

characterized by compromised systolic and diastolic functions that ultimately result in insufficient cardiac output to fulfill systemic metabolic requirements.[1–3] Although drug therapies and mechanical approaches have improved considerably, HF remains a leading cause of death globally, with persistently high morbidity and mortality.[4] The prognosis is especially poor in the elderly and those with comorbid metabolic diseases.[5,6] The pathogenesis of HF is complex, involving multiple pathological processes such as myocardial cell injury, fibrotic remodeling, energy metabolism disorders, and chronic inflammation.[7] Among them, excessive activation of oxidative stress (OS) and inflammatory responses is considered a key factor driving myocardial cell apoptosis and ventricular remodeling.[8] As primary OS mediators, reactive oxygen species (ROS) have dual roles in HF: maintaining cellular homeostasis physiologically, while pathologically activating nuclear factor kappa-light-chain-enhancer of activated B cells (NF-κB)/NOD-like receptor family pyrin domain containing 3 (NLRP3) inflammasomes to promote pro-inflammatory cytokine production, including interleukin 1β (IL-1β) and interleukin 18 (IL-18), and cardiac damage.[9–11] NF-κB, a key transcription factor downstream of ROS, induces the expression of various inflammatory factors, such as tumor necrosis factor-α (TNF-α) and interleukin 6 (IL-6),[12] while the assembly of the NLRP3 inflammasome further amplifies the inflammatory response.[13,14] Accumulating evidence indicates that pharmacological blockade of the NF-κB/NLRP3 signaling axis exerts cardioprotective effects in experimental models of myocardial ischemia-reperfusion, significantly attenuating inflammatory damage and enhancing cardiac performance.[15] However, the exact molecular interactions and control points in the ROS-NF-κB/NLRP3 signaling cascade require further clarification, which currently restricts therapeutic optimization for HF.

In recent years, the LIM domain kinase (LIMK) family, as a core molecular regulator of actin cytoskeleton dynamics, has received increasing attention in cardiovascular diseases.[16] As a serine/threonine-specific protein kinase, LIMK1 modulates cytoskeletal dynamics through cofilin phosphorylation, thereby influencing cellular architecture, motility, and intracellular signaling pathways.[17] Existing studies have demonstrated LIMK1's involvement in multiple cellular processes, including neuronal differentiation, regulation of contractile function, and the pathogenesis of cardiac fibrotic remodeling.[18,19] For example, in an angiotensin II (Ang II)-induced myocardial hypertrophy model, LIMK1 expression was significantly upregulated, and the absence of LIMK1 downregulated the RNA and protein levels of myocardial hypertrophy markers, restoring normal myocardial cell morphology.[20] Additionally, in cardiac tissue from a mouse myocardial infarction model, LIMK1 expression increased and was positively correlated with fibrosis markers (collagen I/III), suggesting that LIMK1 may trigger or promote cardiac fibrosis after myocardial infarction.[21] Research by Su et al demonstrated that LIMK1 knockdown attenuates OS and inflammatory responses, leading to improved cardiac function and ameliorated ventricular remodeling in a rat model of chronic heart failure (CHF).[22] While previous investigations have established LIMK1's involvement in heart failure pathogenesis, the precise molecular mechanisms underlying its regulation of ROS-dependent NF-κB/NLRP3 inflammatory signaling and subsequent cardiomyocyte damage require further elucidation.

This study aimed to explore the role of LIMK1 in ROS-mediated NF-κB/NLRP3 pathway activation and its impact on myocardial cell inflammatory injury and HF, and systematically elucidate the molecular mechanism by which LIMK1 regulates the inflammatory response, thereby providing theoretical support and potential targets for the precise treatment of HF.

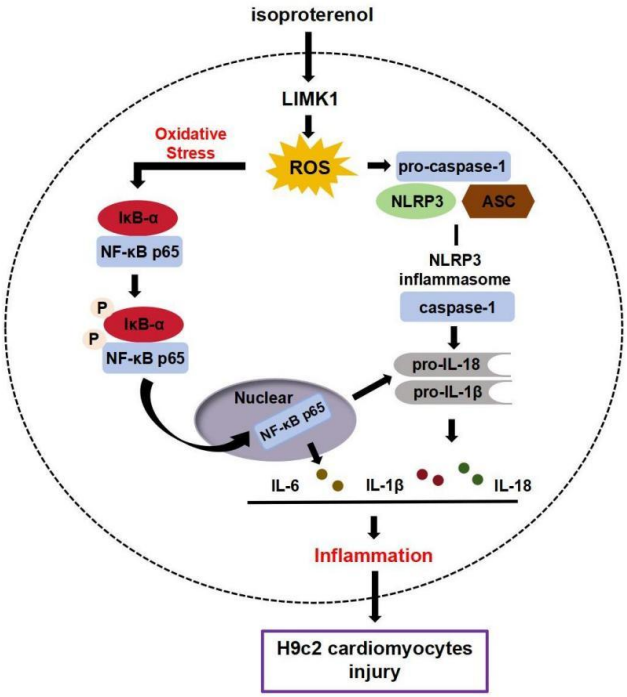

Graphical Abstract.

MATERIALS AND METHODS

Cell Culture

The H9c2 cardiomyocyte cell line was obtained from the Cell Resource Center of Chinese Academy of Medical Sciences. Cell cultures were maintained in DMEM (11965092, Thermo) supplemented with 10% FBS (A5256701, Gibco) and 1% antibiotic-antimycotic solution (15240112, Gibco). Cells were incubated at 37°C in a humidified atmosphere containing 5% CO_2, with routine subculturing performed every 2 to 3 days. Cells were cultured in DMEM without serum containing 10 μM isoproterenol (ISO, I0600000, Sigma) for 48 hours to establish the HF model.[23]

siRNA Transfection

Small interfering RNA (siRNA)-mediated *LIMK1* knockdown was achieved using GenePharma-synthesized si-*LIMK1*, with negative control siRNA (si-NC) as the control. H9c2 cells at 60% to 70% confluence in 6-well plates were transfected with 50 nM siRNA using Lipofectamine 3000/Opti-MEM complexes (Gibco). After 6 hours, the medium was changed to complete DMEM, and cells were harvested 48 hours post-transfection for Western blot validation.

Experimental Design

To comprehensively evaluate the cardioprotective mechanisms of *LIMK1* knockdown against ISO-induced cellular injury, we designed the following experimental groups: (1) Untreated control group (normal culture conditions); (2) ISO-injury model group (10 μM ISO exposure for 48 hours); (3) ISO + si-NC group: treated with ISO after transfection with negative control siRNA; (4) ISO + si-*LIMK1* group: treated with ISO after transfection with si-*LIMK1*. (5) Ang II at a concentration of 1 μmol/L was applied for 48 hours.

To further clarify the mechanism by which *LIMK1* silencing alleviates ISO-induced H9c2 cardiomyocyte injury by regulating ROS and the NF-κB/NLRP3 signaling pathway, 2 additional intervention groups were set up based on the original 4 groups: (5) ISO + si-*LIMK1* + H_2O_2 group: treated with ISO and H_2O_2 (1 mM, ROS agonist, 7722-84-1, Sigma) after transfection with *LIMK1* siRNA for 48 hours; (6) ISO + si-*LIMK1* + dipro group: treated with ISO and diprovocim (dipro; 5 μM, NF-κB agonist, SML2522, Sigma) after transfection with *LIMK1* siRNA for 48 hours; (7) ISO + si-*LIMK1* + Mito-TEMPO group: following transfection with *LIMK1* siRNA, the cells

Published by Tehran University of Medical Sciences (http://ijaai.tums.ac.ir)

were co-treated with ISO and Mito-TEMPO (40 μM; a ROS inhibitor, HY-112879, MCE) for 48 hours.

To examine how ROS inhibition modulates the NF-κB/NLRP3 pathway and mitigates ISO-induced damage in H9c2 cells, 4 experimental conditions were established: (1) Untreated control; (2) ISO-treated group; (3) ISO + NAC group: cells exposed to ISO along with the ROS scavenger N-acetylcysteine (NAC; 5 mM) for 48 hours; (4) ISO + NAC + dipro group: cells treated with ISO, NAC, and dipro for the same duration. Post-treatment samples were then subjected to further analysis. To ensure the reliability of the results, all experiments were independently repeated 3 times (n=3). Each experiment included 5 replicate wells, and the data were statistically analyzed using the average value of the 5 replicate wells as the representative value for that experiment.

Cell Viability Assay

Cellular viability was quantitatively evaluated using a Cell Counting Kit-8 (CCK-8, CA1210, Solarbio). Cells were plated in 96-well plates (3×10^3 cells/well) and allowed to adhere for 24 hours prior to experimental treatments. Following interventions, 10 μL of CCK-8 reagent was added per well, and the plates were incubated at 37°C for 2 hours. Optical density at 450 nm was determined using a Tecan Infinite M200 microplate reader. Results were normalized to untreated controls (set as 100% viability) and expressed as relative viability percentages.

EdU Assay for Cell Proliferation

The proliferative capacity of H9c2 cardiomyocytes was quantitatively analyzed using a commercial 5-ethynyl-2'-deoxyuridine (EdU) detection kit (C0075S, Beyotime). H9c2 cells were seeded on glass coverslips in 24-well plates and incubated with 10 μM EdU for 2 hours under normal growth conditions. Following fixation with 4% PFA (15 minutes) and permeabilization with 0.3% Triton X-100 in PBS (10 minutes), cells were subjected to the Click-iT reaction (100 μL/well, 30 minutes, dark). Nuclei were stained with DAPI for 5 minutes. Cells were then observed and imaged using a fluorescence microscope (CKX53, Olympus), and 5 fields were randomly selected to calculate the percentage of EdU-positive cells (red fluorescence) relative to the total number of cells (blue fluorescence).

Biochemical Assays

After treatment of the H9c2 cells, lysis was performed by adding 0.1 mL of lysis buffer (P0013, Beyotime) per 1 million cells. The samples were centrifuged (12 000g for 10 minutes), and the resulting supernatant was collected for further analysis. Myocardial injury biomarkers were quantified using commercial kits for LDH (C0016, Beyotime) and CK-MB (SEKR-0059, Solarbio) following the manufacturers' protocols. Sample aliquots were incubated with specific reagents, and absorbance was measured at characteristic wavelengths (490 nm for LDH, 450 nm for CK-MB) using a microplate reader. Oxidative stress parameters including malondialdehyde (MDA, S0131S, Beyotime), superoxide dismutase (SOD, S0101S, Beyotime), adenosine triphosphate (ATP, BC0300, Solarbio), and glutathione peroxidase (GSH-Px, BC1195, Solarbio) were similarly assessed at 532 nm, 450 nm, and 412 nm, respectively. Caspase-1 activity was measured using a caspase-1 activity assay kit (C1101, Beyotime) by detecting absorbance at 405 nm.

WGA and Phalloidin Staining

H9c2 cells were analyzed using wheat germ agglutinin (WGA) staining. After PBS washing, samples were fixed, permeabilized, and blocked with 5% BSA (30 minutes). Subsequently, cells were stained with FITC-labeled WGA (5 μg/mL, W849, Invitrogen) for 1 hour at room temperature. Cells were observed and imaged under a fluorescence microscope using a 40× objective lens, and the cellular surface area was quantified with ImageJ software to evaluate the extent of cardiomyocyte hypertrophy. For cytoskeletal visualization, cells were processed identically to the WGA staining protocol before incubation with iFluor™ 594-conjugated phalloidin (5 μg/mL, 40786ES75, Yeasen) for 20 minutes at room temperature under light-protected conditions. Following PBS washes, nuclei were counterstained with DAPI (1:1000, 10236276001, Sigma) for 5 minutes. Cell morphology was examined under a microscope using a 40× objective lens. The surface area of F-actin-stained cells was measured with ImageJ software, normalized to that of the control group (set as 1), and the relative cell surface area (%) of each treatment group was calculated. The above procedures were based on 3 independent biological replicates, and image acquisition and quantitative analysis were performed in a blinded manner, with microscopic

imaging parameters kept constant throughout the experiments.

ROS Level Detection

Intracellular ROS production was measured using 6-Carboxy-2',7'-dichlorodihydrofluorescein diacetate (DCFH-DA, C400, Invitrogen) at a working concentration of 20 μM. Following treatment, cells were PBS-washed twice and incubated with DCFH-DA (37°C, 20 minutes, dark). After 3 washes with serum-free medium, fluorescence microscopy was performed immediately.

Cells were treated with MitoSOX Red (5 μM, M36007, Invitrogen) at 37°C for 10 minutes (dark conditions) after PBS washing. Following additional PBS washes, fluorescence microscopy was conducted. Five fields of view were randomly selected, and fluorescence intensity was analyzed using ImageJ software, with the fluorescence intensity being proportional to the level of mitochondrial ROS. The results were expressed as relative fluorescence intensity, with the control group set to 1.

Mitochondrial Membrane Potential Detection

Mitochondrial membrane potential was measured using JC-1 (10 μg/mL, T3168, Invitrogen). Cells were stained (30 minutes, 37°C), washed, and imaged (BX600, Olympus). The red/green fluorescence ratio was calculated, with lower values indicating mitochondrial depolarization.

qRT-PCR

Total RNA isolation was performed using TRIzol reagent (T9424, Sigma) following the manufacturer's protocol. RNA quality was verified by spectrophotometric analysis (DS-11+, DeNovix) demonstrating A260/A280 ratios ranging from 1.8 to 2.0. Reverse transcription of 1 μg total RNA was carried out using a commercial kit (RR092, Takara). Quantitative PCR analysis was conducted on an ABI 7500 Fast Real-Time PCR System (Thermo) with SYBR Green master mix (CN830A, Takara). Gene-specific primers (Sangon Biotech) were designed as detailed in Table 1. Relative gene expression was normalized to GAPDH.

Flow Cytometry

Cell apoptosis was evaluated using Annexin V-APC/PI double staining (E-CK-A217, Elabscience).[24] After treatment, cells (2×10^5 cells) were collected, PBS-washed, and resuspended in binding buffer (100 μL). Samples were then stained with Annexin V-APC and PI (5 μL each, 15 minutes, RT, dark) before dilution with 400 μL buffer for immediate flow cytometric analysis.

ELISA

Culture supernatants were collected and centrifuged (1000*g* for 10 minutes at 4°C) to remove cellular debris. Inflammatory cytokine concentrations (IL-6, IL-1β, TNF-α, MCP-1) were quantified using commercial ELISA kits (Solarbio: SEKR-0005, SEKR-0002, SEKR-0009, SEKR-0024) following manufacturer protocols. Briefly, samples were incubated in antibody-coated wells (37°C, 1 hour), followed by enzyme conjugate (37°C, 30 minutes) and TMB substrate (room temperature, 10 to 15 minutes, dark). Reactions were terminated and absorbance measured at 450 nm, with cytokine concentrations determined from standard curves.

Immunofluorescence

The treated H9c2 cells were PBS-washed and fixed with 4% PFA for 30 minutes at room temperature. After permeabilization with 0.5% Triton X-100 (20 minutes) and blocking with 5% BSA (30 minutes), cells were incubated overnight at 4°C with the following primary antibodies: anti-8-OHdG (1:100, bs-1278R, Bioss), anti-Cofilin (1:200, 10960-1-AP, Proteintech), anti-NF-κB p65 (2 μg/mL, ab16502, Abcam), and anti-NLRP3 (1:50, ab283819, Abcam). Following PBST washes, Alexa Fluor-conjugated secondary antibodies (1:200, ab150077, Abcam) were applied (1 hour, 37°C). Nuclei were counterstained with DAPI before confocal imaging (TCS SP8, Leica). Quantitative analysis of fluorescence intensity and colocalization was performed using ImageJ.

Western Blot

Following treatment, cellular proteins were extracted using RIPA lysis buffer with 30-minute incubation on ice. Lysates were centrifuged at 12 000 rpm for 15 minutes at 4°C to obtain soluble protein fractions. Protein concentrations were quantified, and equal amounts (20 to 30 μg) were resolved by SDS-PAGE, followed by electrophoretic transfer to PVDF membranes. To control for batch variation, all samples from the groups compared within the same experiment were subjected to electrophoresis on the same gel and

Published by Tehran University of Medical Sciences (http://ijaai.tums.ac.ir)

transferred and incubated on the same membrane. After 1-hour blocking with 5% BSA, membranes were probed with primary antibodies at 4°C overnight. The primary antibodies used in this study (all at 1:1000 dilution unless specified) included: From Cell Signaling Technology: LIMK1 (#3842), Cofilin (#5175), p-Cofilin (#3313), Bax (#2772), Bcl-2 (#28150), cleaved caspase-3 (#9664), Caspase3 (#9662), NF-κB p65 (#8242), p-NF-κB p65 (#3033), IκB-α (#9242), p-IκB-α (#2859), Cleaved-caspase-1 (#9661), Caspase-1 (#83383), OPA1 (#80471), DRP1 (#8570), phospho-DRP1 (#4867), PINK1 (#85325), and Parkin (#32833), and GAPDH (#5174). From Abcam: ANP (ab225844), BNP (1:500, ab19645), β-MHC (MYH7, ab172967), F-actin (1:500, ab205), α-SMA (1 μg/mL, ab7817), Collagen I (ab270993), TGF-β1 (ab215715), NOX2 (1:500, ab310338), NOX4 (ab133303), NLRP3 (ab263899), ASC (ab309497), IL-1β (ab283818), and IL-18 (0.3 μg/mL, ab191860).

The membranes were subjected to three 10-minute washes with TBST, followed by incubation with HRP-linked secondary antibodies (ab6721, ab205719; 1:5000 dilution) at room temperature for 60 minutes. Following additional TBST washes, protein bands were visualized using ECL substrate (P0018, Beyotime) and captured digitally. ImageJ software was used to analyze the gray-scale values of protein bands, with GAPDH serving as the internal reference protein. The relative expression level of the target protein was calculated as the ratio of the target protein's gray-scale value to that of the internal reference protein. For standardized presentation, the relative expression level of the target protein in the control group was used as the reference for data normalization. The processed data were visualized as bar charts.

Statistical Analysis

Prior to statistical testing, the normality of data in each group was assessed using the Shapiro–Wilk test, and homogeneity of variance was evaluated using Levene's test. For comparisons between 2 groups that met the assumptions of normal distribution and homoscedasticity, Student's t-test was applied; for multiple-group comparisons, one-way ANOVA followed by the Bonferroni post hoc test was used. When the data did not conform to a normal distribution or showed significant heterogeneity of variance, appropriate nonparametric tests were performed (the Mann–Whitney U test for two-group comparisons, and the Kruskal–Wallis test with corresponding post hoc analyses for multiple-group comparisons). Statistical significance was set at $p<.05$. For experiments such as ELISA and Western blot performed across multiple batches, "batch" was incorporated as a covariate/factor into the model to assess and control for potential batch effects. Key data were analyzed using two-way ANOVA (group + batch) or linear mixed-effects models, with results reported as adjusted means ± SEM. To minimize observer bias, all data analyses were conducted in a blinded manner, with the investigators unaware of the specific treatment allocation throughout the quantification process. No outliers were artificially excluded in this study; all experimental data that met the predefined inclusion criteria were included in the statistical analyses.

RESULTS

Silencing *LIMK1* Alleviates ISO-Induced Injury in H9c2 Cardiomyocytes

The H9c2 cell line, a subclone originating from rat embryonic cardiac tissue, serves as a well-established in vitro model for cardiovascular research.[25,26] In this study, H9c2 cardiomyocyte injury was induced by ISO. The results showed that cell viability gradually decreased with increasing ISO concentrations (Figure 1A). Based on these findings, treatment with 10 μM ISO for 48 hours was selected as the experimental condition for subsequent assays. Based on the preliminary experimental results, we ultimately chose 10 μM ISO for 48 hours to establish a heart failure cell model and to investigate the role of LIMK1 in ISO-induced H9c2 cardiomyocyte injury. Immunofluorescence, qRT-PCR, and immunoblot analyses consistently demonstrated that ISO stimulation significantly enhanced LIMK1 expression in H9c2 cardiomyocytes (Figure 1B–F), confirming ISO's ability to potently upregulate LIMK1 in these cells. This suggests that LIMK1 may act as a stress response molecule involved in the injury mechanism of cardiomyocytes during HF. To investigate LIMK1's functional role, we performed siRNA-mediated knockdown in H9c2 cells, with immunoblot analysis confirming successful suppression of LIMK1 protein levels in si-*LIMK1*-transfected groups (Figure 1G–H), thereby establishing a cell model with low LIMK1 expression and providing a reliable experimental foundation for subsequent functional studies.

HF leads to cardiomyocyte hypertrophy, structural disarray, energy metabolism dysfunction, increased apoptosis and necrosis, and since proliferation ability is extremely low, it cannot effectively repair damage, ultimately resulting in decreased cardiac function and fibrotic remodeling.[27,28] Microscopic observation showed that ISO treatment induced morphological changes in some H9c2 cells (Figure 1I). Both CCK-8 and EdU incorporation assays revealed that ISO exposure markedly impaired the viability and proliferation of H9c2 cardiomyocytes (Figure 1J–L). LDH and CK-MB, as important biomarkers of myocardial injury, directly reflect the integrity and damage of the cardiomyocyte membrane.[29,30] Following ISO stimulation, H9c2 cells exhibited a marked elevation in LDH and CK-MB release (Figure 1M–N). While no notable changes were observed between the ISO + si-NC and ISO-treated groups, knockdown of LIMK1 substantially attenuated ISO-induced cellular injury. This protective effect was demonstrated by improved cell morphology, elevated viability, enhanced proliferation, and reduced leakage of LDH and CK-MB. These results confirm that *LIMK1* silencing can alleviate ISO-induced injury in H9c2 cardiomyocytes.

Silencing of *LIMK1* Reduces ISO-Induced Hypertrophy, Fibrosis, and Apoptosis in H9c2 Cardiomyocytes

This study comprehensively elucidates the regulatory function and underlying mechanisms of LIMK1 in ISO-mediated cardiomyocyte hypertrophy, fibrosis, and apoptosis through multiple experimental approaches, including WGA staining, phalloidin staining, qRT-PCR, flow cytometry, and Western blot analysis. WGA staining revealed that Ang II and ISO treatment significantly increased the surface area of cardiomyocytes (Figure 2A–D). In addition, qRT-PCR and Western blot analyses revealed that the expression levels of the myocardial hypertrophy markers ANP, BNP, and β-MHC were significantly upregulated following ISO treatment. These changes showed no significant differences in the si-NC control group but were significantly improved in the LIMK1-silenced group (Figure 2E–G). As a key kinase regulating actin dynamics, LIMK1 promotes F-actin polymerization and stress fiber formation by phosphorylating its downstream effector, Cofilin. This process is critically involved in the pathological remodeling of cardiomyocytes.[31] Cytochalasin staining revealed that ISO treatment markedly enlarged cardiomyocyte surface area relative to controls, whereas *LIMK1* knockdown effectively reversed this hypertrophic response (Figure 2J–K). Complementary Western blot data showed that ISO stimulation substantially enhanced Cofilin phosphorylation and F-actin expression (Figure 2L–O). Importantly, *LIMK1* silencing suppressed both Cofilin activation and F-actin accumulation, demonstrating its regulatory function in cardiomyocyte hypertrophy.

The study also found that silencing LIMK1 had a significant inhibitory effect on myocardial fibrosis and cell apoptosis. TGF-β and ISO stimulation markedly elevated the expression of fibrotic markers (α-SMA, Collagen I, and TGF-β1), while *LIMK1* knockdown effectively suppressed these pro-fibrotic mediators (Figure 2H–I, P–Q). Flow cytometry analysis demonstrated a significant increase in apoptosis following ISO exposure (Figure 2R–S). Corresponding Western blot results showed elevated Bax expression, reduced Bcl-2 levels, and enhanced caspase-3 activation, collectively indicating enhanced apoptotic signaling (Figure 2T–U). Importantly, *LIMK1* silencing effectively reversed these abnormal changes in apoptosis-related markers.

Silencing of *LIMK1* Reduces ISO-Induced ROS Production, Mitochondrial Damage, and Inflammatory Injury in H9c2 Cardiomyocytes

To explore the key role of LIMK1 in regulating the OS response induced by ISO in H9c2 cardiomyocytes, DCFH-DA staining revealed that ISO treatment significantly increased intracellular ROS levels, while 8-OHdG immunofluorescence signals were significantly enhanced, indicating exacerbated DNA oxidative damage in cardiomyocytes (Figure 3A–C). Biochemical analysis revealed that ISO treatment substantially increased MDA levels while decreasing SOD and GSH-Px activities in H9c2 cells, confirming ISO-induced OS (Figure 3D–F). Consistent with these findings, Western blotting detected elevated expression of ROS-generating enzymes NOX2 and NOX4 after ISO exposure (Figure 3G–H). While no alterations were observed in the ISO + si-NC group, *LIMK1* knockdown effectively normalized these OS parameters.

To assess LIMK1's impact on mitochondrial homeostasis and inflammation, we performed MitoSOX and JC-1 staining assays. ISO treatment markedly elevated mitochondrial ROS generation and decreased

the JC-1 red/green ratio, indicating impaired membrane potential (Figure 3I–L). These effects remained unaltered in the ISO + si-NC group. Notably, *LIMK1* silencing substantially attenuated mitochondrial ROS accumulation and restored membrane potential, demonstrating its protective role in mitochondrial function.

ELISA analysis demonstrated that ISO treatment markedly enhanced the secretion of pro-inflammatory mediators (IL-6, IL-1β, TNF-α, and MCP-1) (Figure 3M–P), while *LIMK1* knockdown substantially suppressed their release. These findings suggest that LIMK1 plays a pivotal role in regulating ISO-induced inflammatory responses in cardiomyocytes. Western blotting and related assay kits further showed that *LIMK1* silencing markedly reduced ISO-induced DRP1 phosphorylation, while significantly upregulating OPA1, PINK1, and PRKN expression as well as ATP content (Figure 3Q–T). These findings suggest that *LIMK1* may participate in ISO-induced cardiomyocyte injury by modulating OS, mitochondrial dysfunction, and inflammatory responses.

Silencing of *LIMK1* Alleviates ISO-Induced H9c2 Cardiomyocyte Injury by Inhibiting ROS

To elucidate the mechanism underlying LIMK1-mediated protection against ISO-induced cardiomyocyte injury, 6 experimental groups were established: Control, ISO, ISO + si-NC, ISO + si-*LIMK1*, ISO + si-*LIMK1* + H_2O_2, and ISO + si-*LIMK1* + Mito-TEMPO. First, we confirmed that treatment with 1 mM H_2O_2 exerted no obvious cytotoxicity (Figure 4A). DCFH-DA assays revealed that ISO treatment substantially increased intracellular ROS levels, whereas *LIMK1* knockdown effectively attenuated this OS response. However, when H_2O_2 (a ROS agonist) was added to the *LIMK1* silencing group, ROS levels significantly increased again (Figure 4B–C). This trend was also reflected in OS indicators: MDA content was significantly increased in ISO-treated H9c2 cardiomyocytes, while SOD and GSH-Px levels were significantly reduced. Silencing *LIMK1* effectively reversed these changes, but H_2O_2 treatment partially counteracted this protective effect (Figure 4D–F). Evaluation of myocardial injury markers revealed that ISO treatment substantially elevated LDH and CK-MB release in H9c2 cardiomyocytes. While *LIMK1* knockdown significantly attenuated this effect, subsequent H_2O_2 exposure reversed the cardioprotection (Figure 4G–H). In addition, Mito-TEMPO treatment further enhanced the antioxidant effect of si-*LIMK1*.

Cytochalasin staining demonstrated that ISO treatment induced cardiomyocyte enlargement, which was attenuated by *LIMK1* knockdown but partially restored upon H_2O_2 exposure (Figure 4I–J). Western blot analysis confirmed ISO-induced upregulation of both hypertrophic markers (ANP, BNP, β-MHC) and fibrotic proteins (α-SMA, Collagen I, TGF-β1). *LIMK1* silencing effectively inhibited these abnormal expression changes, but H_2O_2 treatment partially reversed this inhibition (Figure 4K–N). Apoptosis analysis by flow cytometry revealed consistent results: ISO stimulation markedly enhanced H9c2 cell apoptosis, which was attenuated by *LIMK1* knockdown but subsequently restored upon H_2O_2 exposure (Figure 4O–P). In addition, Mito-TEMPO treatment further potentiated the inhibitory effects of si-*LIMK1* on cardiac hypertrophy and fibrosis, as well as on cell apoptosis

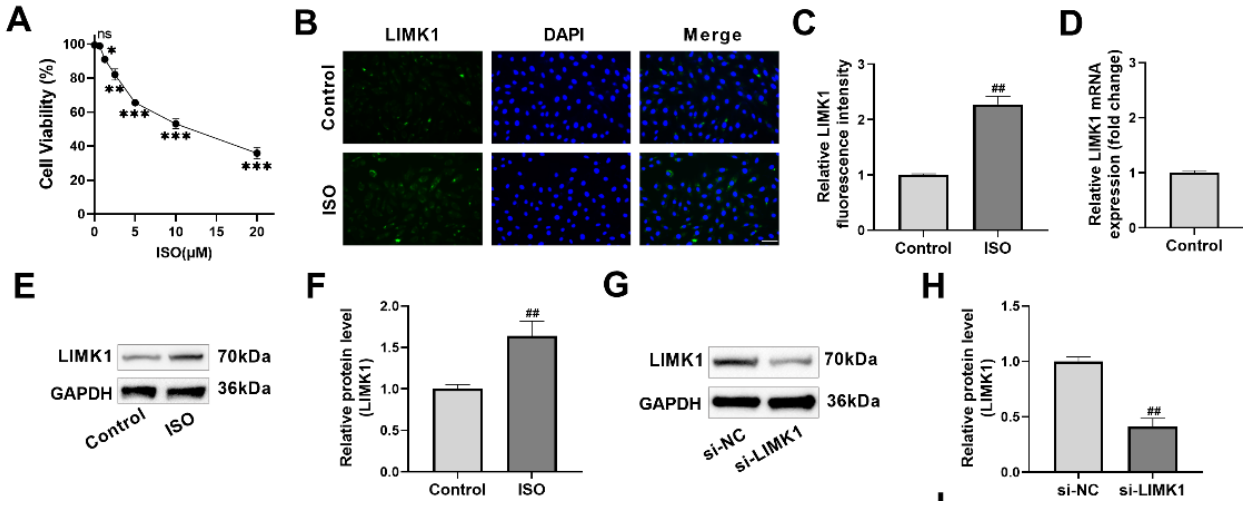

Published by Tehran University of Medical Sciences (http://ijaai.tums.ac.ir)

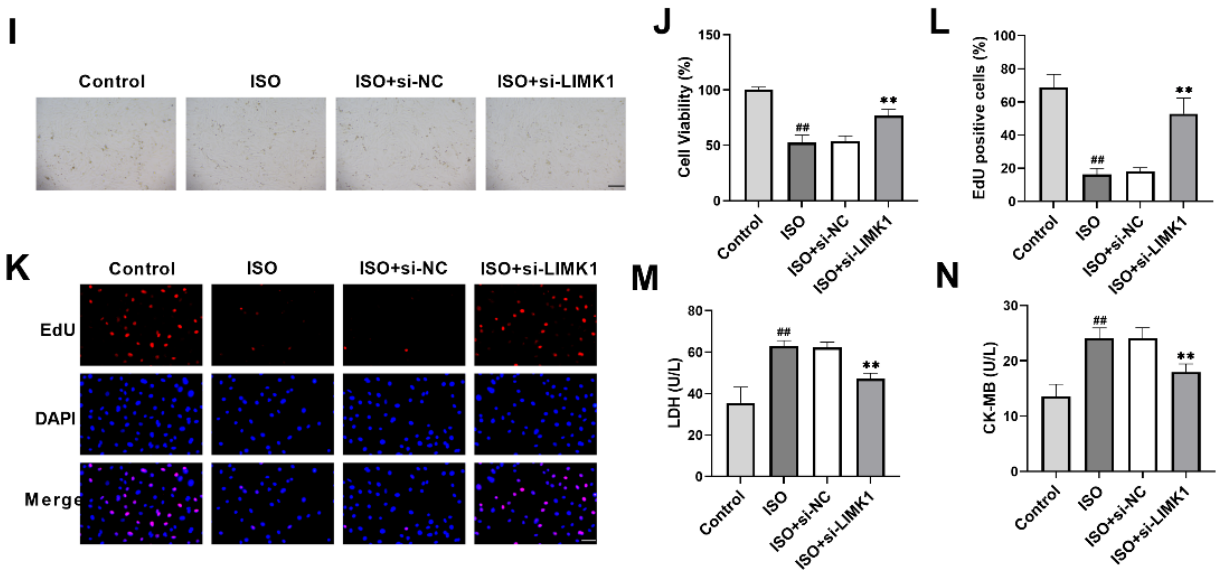

Figure 1. Silencing *LIMK1* alleviates ISO-induced damage in H9c2 cardiomyocytes. A. Cell viability of H9c2 cells treated with different concentrations of ISO for 48 hours was assessed by CCK-8 to determine the optimal induction concentration. ns $p>0.05$, *$p<0.05$, **$p<0.01$, ***$p<0.001$ vs Control; B–F. Immunofluorescence, qRT-PCR, and Western blot were used to detect *LIMK1* expression at the mRNA and protein levels in H9c2 cells following ISO induction (Scale bar 50 μm); G–H. Western blot was performed to verify the transfection efficiency of si-*LIMK1* and to confirm the successful establishment of the *LIMK1* knockdown cell model; I. Morphological changes in each group (Control, ISO, ISO + si-NC, ISO + si-*LIMK1*) were observed under a microscope (Scale bar 200 μm); J–L. CCK-8 and EdU staining were used to evaluate changes in cell viability and proliferative capacity in each group (Scale bar 50 μm); M–N. Biochemical assay kits were used to measure the release levels of the myocardial injury markers LDH and CK-MB in the cell culture supernatant. n=3. $^{\#\#}p<0.01$ vs Control; **$p<0.01$ vs ISO.

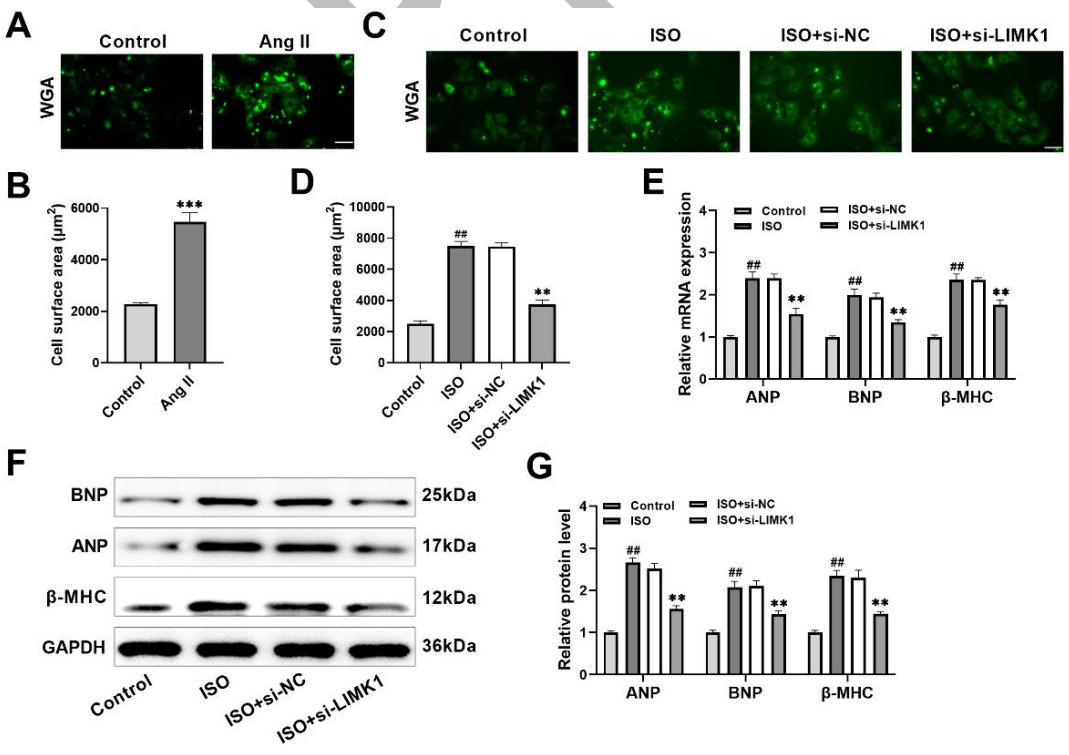

Published by Tehran University of Medical Sciences (http://ijaai.tums.ac.ir)

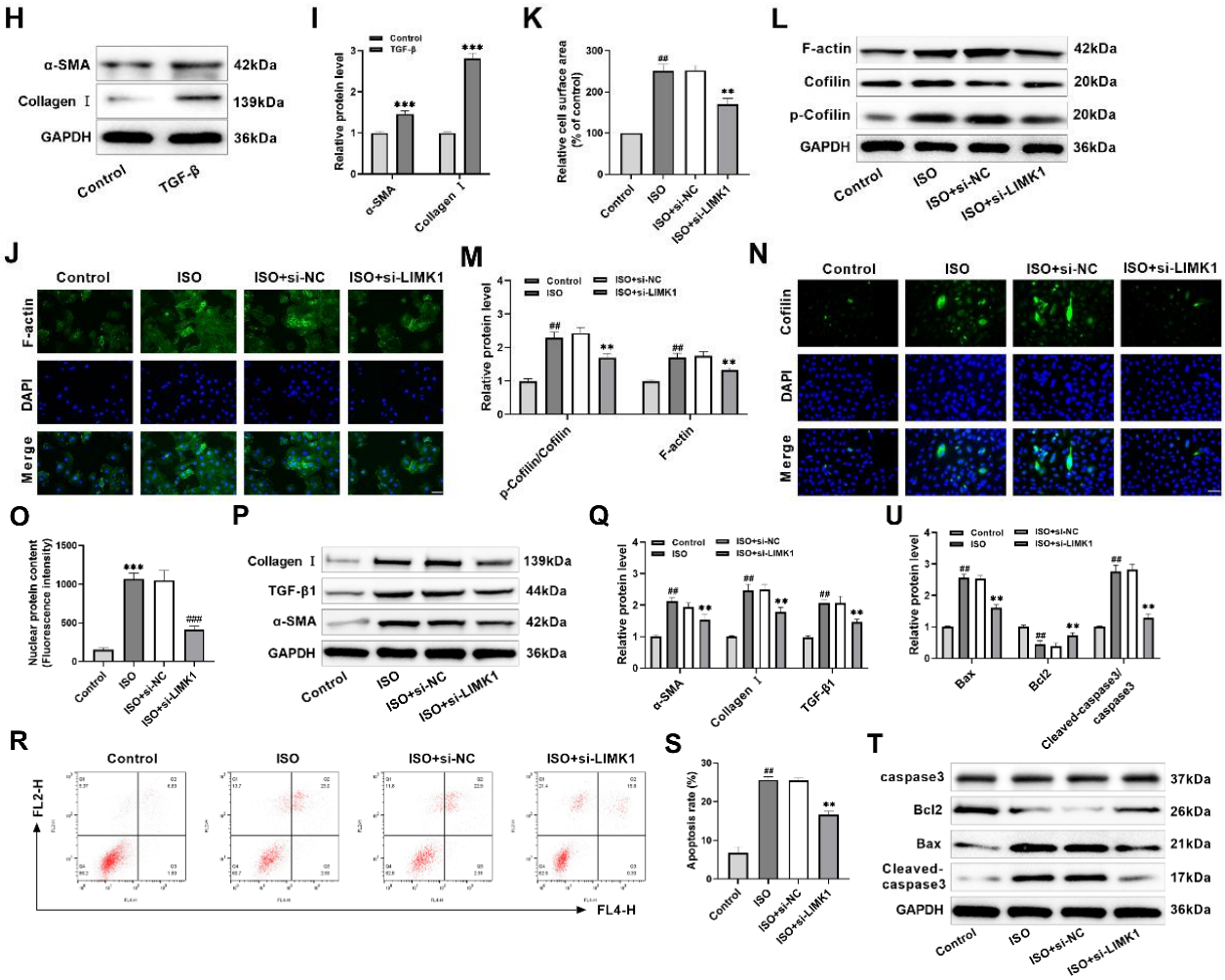

Figure 2. Silencing *LIMK1* alleviates ISO-induced hypertrophy, fibrosis, and apoptosis in H9c2 cardiomyocytes. A–D. WGA staining was used to observe and quantify the cardiomyocyte surface area in each group, thereby assessing the degree of cellular hypertrophy (Scale bar 50 μm); E–G. qRT-PCR and Western blot were employed to determine the expression levels of the hypertrophic markers ANP, BNP, and β-MHC; H–I. Western blot was used to detect the expression of the fibrosis-related proteins α-SMA and Collagen I; J–K. Phalloidin staining was performed to observe cell surface area and microfilament cytoskeletal remodeling (Scale bar 50 μm); L–O. Immunofluorescence and Western blot were used to assess p-Cofilin levels and F-actin protein expression, in order to analyze the regulatory effects of LIMK1 on the cytoskeleton (Scale bar 50 μm); P–Q. Western blot was further conducted to determine the expression of the fibrosis-related proteins α-SMA, Collagen I, and TGF-β1; R–S. Flow cytometry was used to detect and quantify the apoptotic rate of cells in each group; T–U. Western blot was used to examine the activation status of the apoptosis-related proteins Bax, Bcl-2, and Caspase-3. *n*=3. $^{\#\#}p$<0.01 vs Control; **p<0.01 vs ISO.

Published by Tehran University of Medical Sciences (http://ijaai.tums.ac.ir)

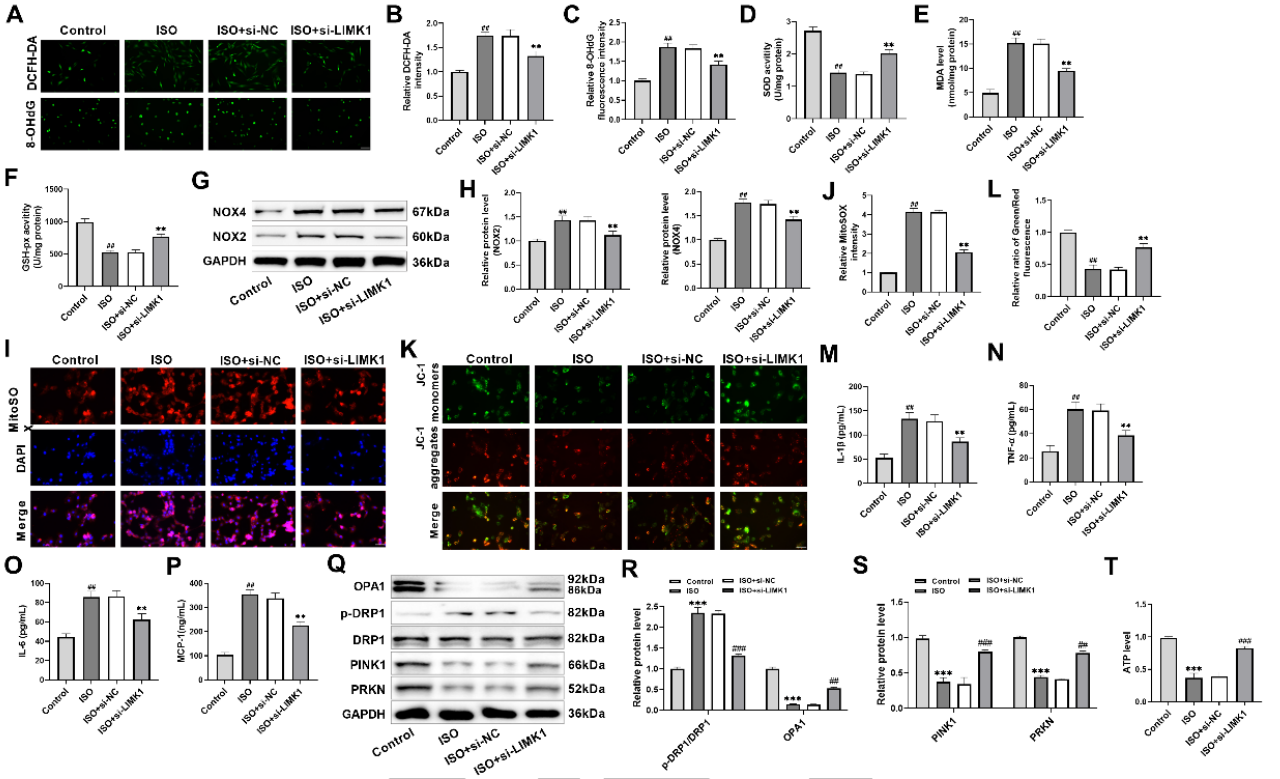

Figure 3. Silencing *LIMK1* reduces ISO-induced ROS production, mitochondrial damage, and inflammatory injury in H9c2 cardiomyocytes. A–C. DCFH-DA staining was used to assess intracellular ROS levels, and 8-OHdG immunofluorescence was applied to evaluate the extent of DNA oxidative damage (Scale bar 100 μm); D–F. Biochemical assay kits were employed to measure the content of the lipid peroxidation product MDA and the activities of the antioxidant enzymes SOD and GSH-Px; G–H. Western blot was used to detect the expression of the ROS-generating proteins NOX2 and NOX4; I–L. MitoSOX staining was performed to detect mitochondrial superoxide production, and JC-1 staining was used to evaluate changes in mitochondrial membrane potential (Scale bar 50 μm); M–P. ELISA was used to determine the concentrations of the proinflammatory cytokines IL-6, IL-1β, TNF-α, and MCP-1 in the cell culture supernatant; Q–T. Western blot was conducted to examine DRP1 phosphorylation and the expression of the mitochondrial dynamics–related proteins OPA1, PINK1, and PRKN, and ATP content was measured to evaluate mitochondrial function. *n*=3. ##*p*<0.01 vs Control; ***p*<0.01 vs ISO.

Silencing of *LIMK1* Alleviates ISO-Induced H9c2 Cardiomyocyte Injury by Inhibiting ROS

To elucidate the mechanism underlying LIMK1-mediated protection against ISO-induced cardiomyocyte injury, 6 experimental groups were established: Control, ISO, ISO + si-NC, ISO + si-*LIMK1*, ISO + si-*LIMK1* + H_2O_2, and ISO + si-*LIMK1* + Mito-TEMPO. First, we confirmed that treatment with 1 mM H_2O_2 exerted no obvious cytotoxicity (Figure 4A). DCFH-DA assays revealed that ISO treatment substantially increased intracellular ROS levels, whereas *LIMK1* knockdown effectively attenuated this OS response. However, when H_2O_2 (a ROS agonist) was added to the *LIMK1* silencing group, ROS levels significantly increased again (Figure 4B–C). This trend was also reflected in OS indicators: MDA content was significantly increased in ISO-treated H9c2 cardiomyocytes, while SOD and GSH-Px levels were significantly reduced. Silencing *LIMK1* effectively reversed these changes, but H_2O_2 treatment partially counteracted this protective effect (Figure 4D–F). Evaluation of myocardial injury markers revealed that ISO treatment substantially elevated LDH and CK-MB release in H9c2 cardiomyocytes. While *LIMK1* knockdown significantly attenuated this effect, subsequent H_2O_2 exposure reversed the cardioprotection (Figure 4G–H). In addition, Mito-TEMPO treatment further enhanced the antioxidant effect of si-*LIMK1*.

Published by Tehran University of Medical Sciences (http://ijaai.tums.ac.ir)

Cytochalasin staining demonstrated that ISO treatment induced cardiomyocyte enlargement, which was attenuated by *LIMK1* knockdown but partially restored upon H_2O_2 exposure (Figure 4I–J). Western blot analysis confirmed ISO-induced upregulation of both hypertrophic markers (ANP, BNP, β-MHC) and fibrotic proteins (α-SMA, Collagen I, TGF-β1). *LIMK1* silencing effectively inhibited these abnormal expression changes, but H_2O_2 treatment partially reversed this inhibition (Figure 4K–N). Apoptosis analysis by flow cytometry revealed consistent results: ISO stimulation markedly enhanced H9c2 cell apoptosis, which was attenuated by *LIMK1* knockdown but subsequently restored upon H_2O_2 exposure (Figure 4O–P). In addition, Mito-TEMPO treatment further potentiated the inhibitory effects of si-*LIMK1* on cardiac hypertrophy and fibrosis, as well as on cell apoptosis.

Silencing of *LIMK1* Alleviates ISO-Induced Inflammatory Injury in H9c2 Cardiomyocytes by Inhibiting the NF-κB/NLRP3 Pathway

This investigation delineates the cardioprotective mechanism of *LIMK1* silencing against ISO-mediated inflammatory damage in H9c2 cardiomyocytes, involving coordinated modulation of the NF-κB/NLRP3 axis. The synergistic interplay between NF-κB and NLRP3 amplifies inflammatory cascades through reciprocal activation.[32] Immunofluorescence and Western blot analyses showed that NF-κB p65 expression was markedly upregulated in the ISO group, accompanied by significant increases in the p-NF-κB-p65/NF-κB-p65 and p-IκB-α/IκB-α ratios (Figure 5A–D), indicating activation of the NF-κB signaling pathway. Further immunofluorescence analysis revealed that ISO treatment markedly enhanced NF-κB p65 nuclear translocation and the fluorescence intensity of NLRP3 (Figure 5E–H), suggesting that ISO strongly induces upregulation of NF-κB and NLRP3 expression. The NLRP3 inflammasome, a crucial innate immune complex comprising NLRP3, ASC, and caspase-1,[33] exhibited elevated expression of its components (NLRP3, ASC) and enhanced caspase-1 cleavage in ISO-treated cells (Figure 5I–J). Importantly, *LIMK1* knockdown suppressed both NF-κB/NLRP3 activation and IκB-α phosphorylation. The expression of inflammasome-related proteins was significantly downregulated, thereby suppressing inflammasome activation. These findings demonstrate that *LIMK1* knockdown modulates myocardial inflammatory responses through NF-κB/NLRP3 signaling pathway regulation.

The above mechanism was further validated by intervention experiments using an NF-κB agonist (dipro), and it was confirmed that 5 μM dipro had no significant effect on cell viability (Figure 5K). ELISA analysis demonstrated elevated secretion of pro-inflammatory cytokines (IL-6, IL-1β, TNF-α, MCP-1) in ISO-stimulated cardiomyocytes, corroborated by Western blot showing upregulated IL-1β and IL-18 expression (Figure 5L–O). *LIMK1* knockdown substantially suppressed this inflammatory response, an effect reversed by NF-κB activation. Similarly, *LIMK1* silencing attenuated NLRP3 inflammasome activation (NLRP3, ASC, cleaved caspase-1 downregulation), while NF-κB agonist treatment restored inflammasome component expression (Figure 5P–S). These findings establish that *LIMK1* inhibition protects against ISO-induced cardiac inflammation through NF-κB/NLRP3 pathway suppression.

Inhibition of ROS Alleviates ISO-Induced H9c2 Cardiomyocyte Injury by Inhibiting NF-κB/NLRP3 Activation

To investigate ROS-mediated regulation of NF-κB/NLRP3 signaling in ISO-induced cardiomyocyte injury, 4 experimental groups were examined: Control, ISO, ISO + NAC (ROS inhibitor), and ISO + NAC + dipro (NF-κB agonist). Western blot analysis revealed that ISO stimulation markedly enhanced phosphorylation of NF-κB p65 and IκB-α, along with increased expression of NLRP3 inflammasome components (NLRP3, ASC, cleaved caspase-1) (Figure 6A–C). ROS inhibition by NAC substantially attenuated these effects, demonstrating ROS's pivotal role in NF-κB/NLRP3 pathway activation. Subsequent NF-κB agonism with dipro reversed NAC's suppressive effects, conclusively establishing ROS-dependent regulation of cardiac injury via the NF-κB/NLRP3 axis.

The LDH assay revealed that ISO stimulation substantially elevated LDH activity in culture supernatants, whereas NAC treatment significantly attenuated this release, demonstrating ROS inhibition's membrane-stabilizing effect. However, when dipro was added to the NAC treatment, the LDH release increased again (Figure 6D). WGA staining demonstrated ISO-induced cardiomyocyte enlargement characteristic of pathological hypertrophy, which was attenuated by NAC treatment but partially restored upon dipro co-

administration (Figure 6E–F). Cytochalasin staining confirmed cardiomyocyte enlargement following ISO treatment, which was effectively mitigated by NAC administration. However, dipro treatment caused the cell surface area to increase again (Figure 6G–H). Western blot analysis of fibrotic markers revealed that ISO stimulation markedly enhanced α-SMA, Collagen I, and TGF-β1 expression, whereas NAC treatment effectively suppressed this fibrotic response. Dipro treatment partially blocked the inhibitory effect of NAC (Figure 6I–J). Flow cytometric analysis revealed ISO-induced cardiomyocyte apoptosis, which was attenuated by NAC treatment. Dipro treatment led to a rebound in the apoptosis rate (Figure 6K–L). Quantification of secreted inflammatory mediators by ELISA demonstrated that ISO treatment markedly elevated extracellular levels of IL-6, IL-1β, IL-18, and MCP-1 in cultured supernatants. NAC treatment inhibited the production of these inflammatory factors, while dipro treatment partially restored the secretion levels of these inflammatory factors (Figure 6M–P). Collectively, these findings demonstrate that ROS-mediated cardiomyocyte dysfunction occurs through NF-κB/NLRP3 pathway activation, as evidenced by multiple cellular injury parameters.

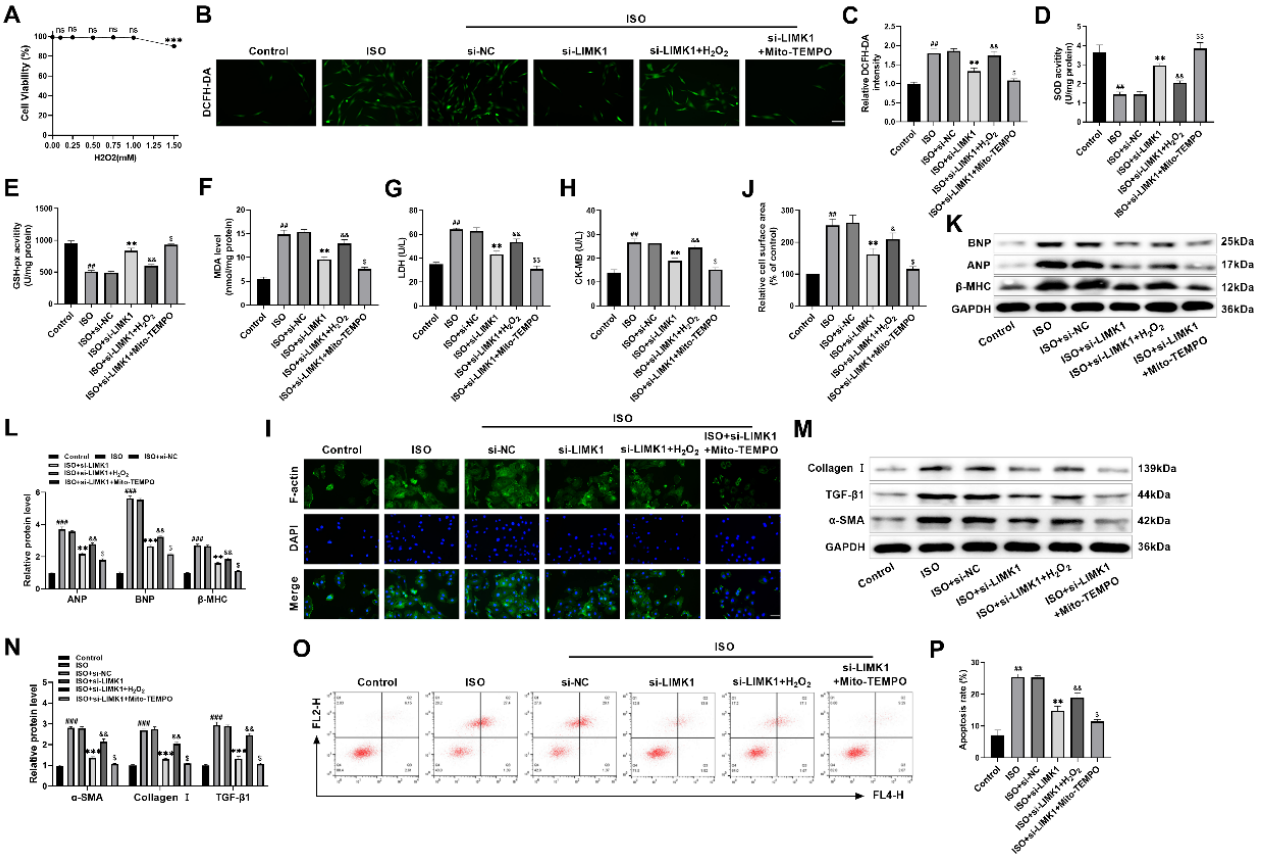

Figure 4. Silencing *LIMK1* alleviates ISO-induced damage in H9c2 cardiomyocytes by inhibiting ROS production. A. CCK-8 assay was used to assess the effect of H_2O_2 (1 mM) on cell viability to verify the safety of the intervention concentration. ns $p>0.05$, ***$p<0.001$ vs Control; B–C. DCFH-DA staining was used to detect changes in intracellular ROS levels in each group after treatment with the ROS agonist (H_2O_2) or scavenger (Mito-TEMPO) (Scale bar 100 μm); D–F. The levels of oxidative stress indicators MDA, SOD, and GSH-Px in each group were measured; G–H. The release of LDH and CK-MB in each group was determined to evaluate the extent of cell injury; I–J. Phalloidin staining was performed to quantitatively analyze changes in cell surface area in each group (Scale bar 50 μm); K–N. Western blot analysis was conducted to determine the expression levels of hypertrophy markers (ANP, BNP, β-MHC) and fibrosis markers (α-SMA, Collagen I, TGF-β1); O–P. Flow cytometry was used to quantitatively analyze the differences in apoptosis rates among the groups. n=3. $^{\#\#}p<0.01$ vs Control; **$p<0.01$ vs ISO; &$p<.05$, $^{\&\&}p<.01$ vs ISO + si-*LIMK1*.

Published by Tehran University of Medical Sciences (http://ijaai.tums.ac.ir)

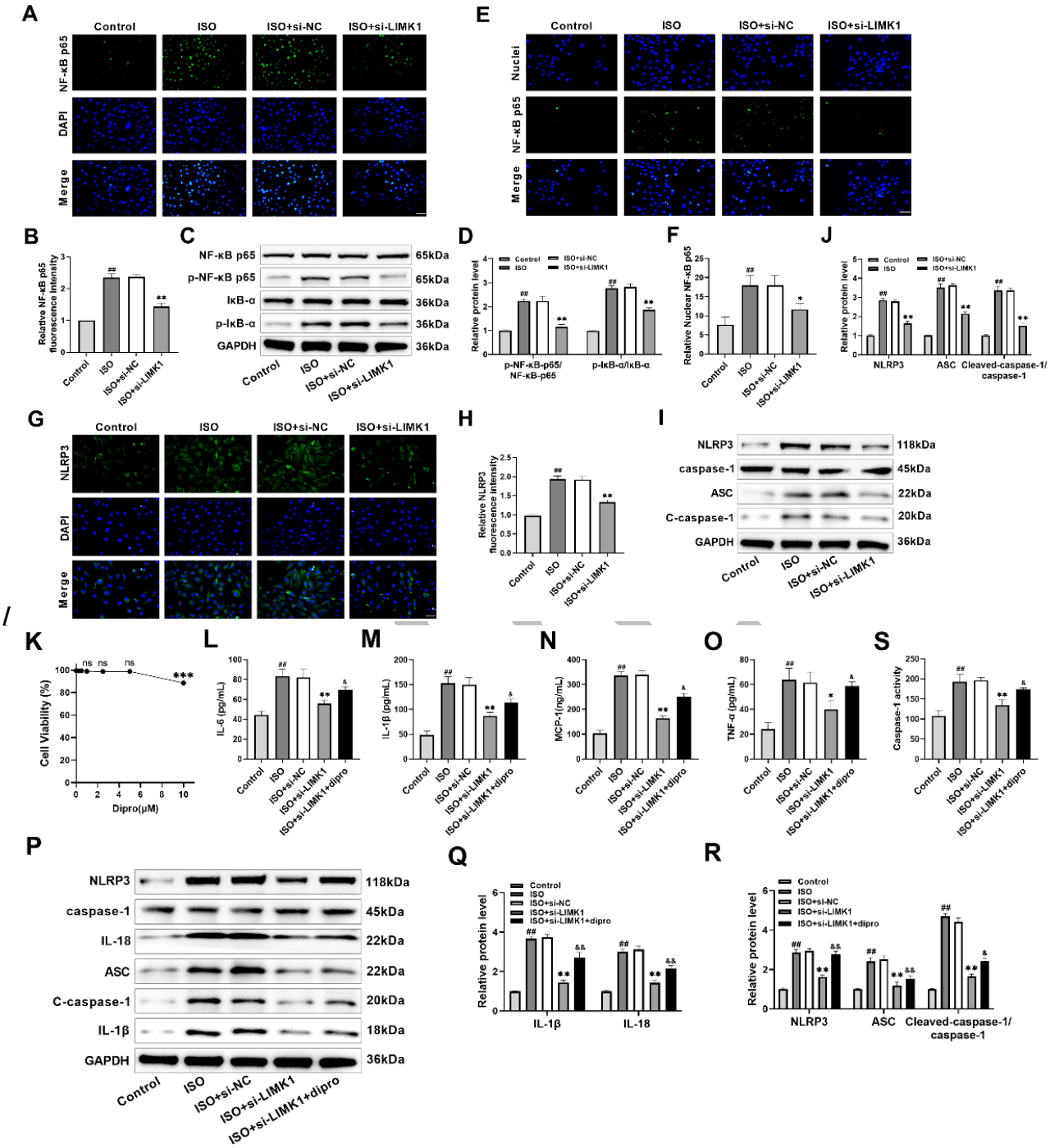

Figure 5. Silencing *LIMK1* alleviates ISO-induced inflammatory injury in H9c2 cardiomyocytes by inhibiting NF-κB/NLRP3. A–D. Western blot analysis of the expression and phosphorylation levels of key proteins in the NF-κB signaling pathway, including p65, p-p65, IκB-α, and p-IκB-α (Scale bar 50 μm); E–H. Immunofluorescence assay to observe the nuclear translocation of NF-κB p65 and changes in NLRP3 fluorescence intensity (Scale bar 50 μm); I–J. Western blot analysis of the expression of inflammasome components, including NLRP3, ASC, and cleaved caspase-1; K. CCK-8 assay to evaluate the effect of the NF-κB agonist dipro on cell viability. ns $p>0.05$, $^{***}p<0.001$ vs Control; L–O. ELISA to determine the concentrations of the pro-inflammatory cytokines IL-6, IL-1β, TNF-α, and MCP-1 in each group; P–S. Western blot analysis of the expression of mature inflammatory cytokines IL-1β and IL-18, as well as NLRP3-related proteins, to assess the antagonistic effect of dipro on the protective role of LIMK1. $n=3$. ns $p>.05$, $^{\#\#}p<0.01$ vs Control; $^{**}p<0.01$ vs ISO; $\&p<0.05$, $^{\&\&}p<0.01$ vs ISO + si-*LIMK1*.

Published by Tehran University of Medical Sciences (http://ijaai.tums.ac.ir)

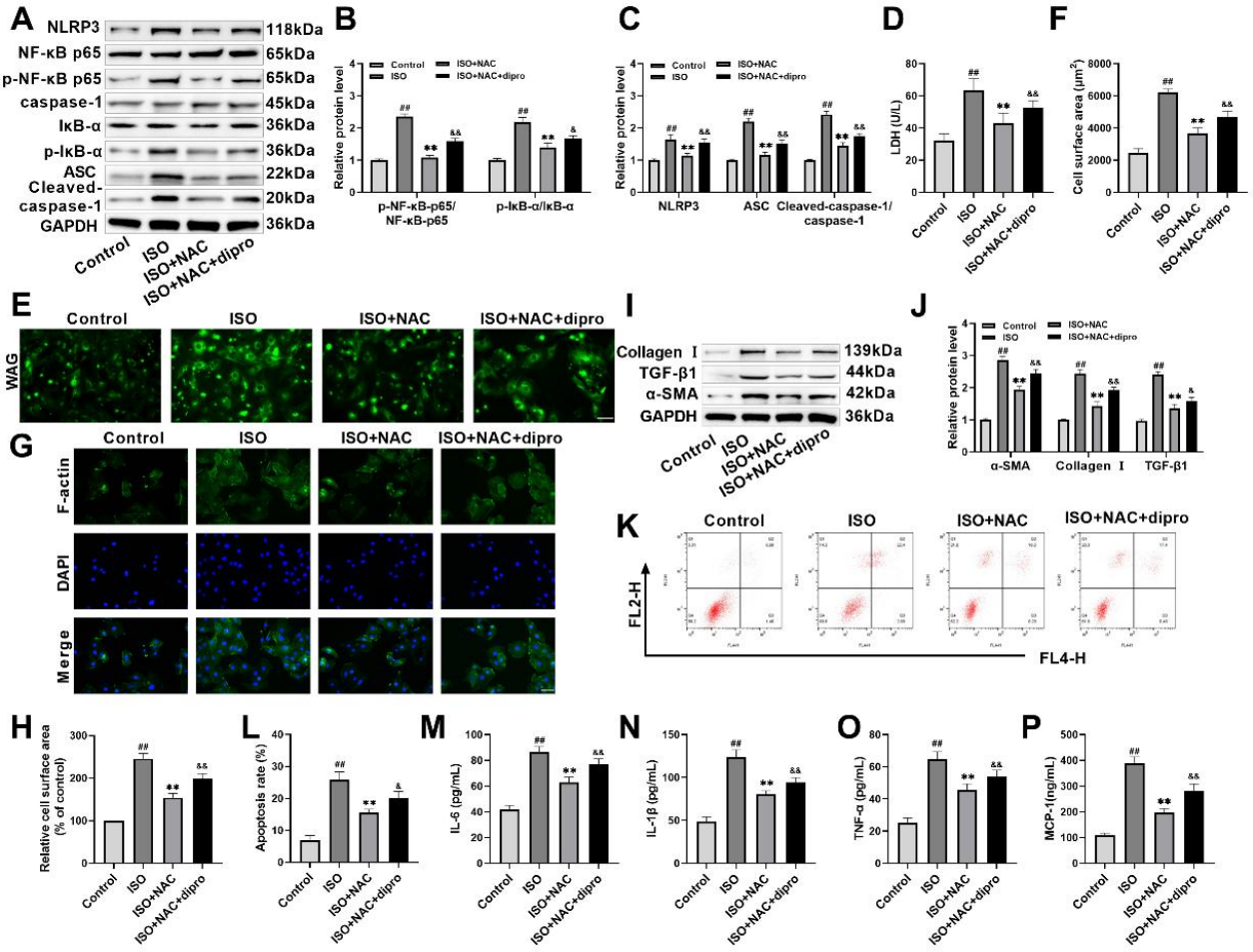

Figure 6. Inhibition of ROS alleviates ISO-induced damage in H9c2 cardiomyocytes by suppressing NF-κB/NLRP3 activation. A–C. Four experimental groups (Control, ISO, ISO + NAC, ISO + NAC + dipro) were established to investigate ROS-mediated NF-κB/NLRP3 activation in ISO-induced injury. Immunoblot analysis examined key pathway components: NF-κB p65 (phosphorylation status), IκB-α (degradation), NLRP3 inflammasome complex formation (ASC, caspase-1 cleavage); D. Cellular damage was quantified by LDH release; E–F. WGA staining visualized hypertrophic morphology (Scale bar 50 μm); G–H. Phalloidin-based morphometry determined cell surface area changes (Scale bar 50 μm); I–J. Fibrotic responses were assessed through α-SMA, Collagen I, and TGF-β1 immunodetection; K–L. Apoptotic rates were measured by flow cytometry; M–P. Inflammatory cytokine secretion (IL-6, IL-1β, IL-18, MCP-1) was quantified via ELISA to validate ROS-NF-κB/NLRP3 axis involvement. *n*=3. ##*p*<0.01 vs Control; ***p*<0.01 vs ISO; &&*p*<0.01 vs ISO + NAC.

DISCUSSION

The LIMK family mainly includes 2 members, LIMK1 and LIMK2, which regulate actin cytoskeletal remodeling by phosphorylating downstream substrates, such as cofilin.[34] LIMK demonstrates broad expression patterns across cardiovascular tissues and participates in modulating critical pathological mechanisms such as endothelial dysfunction, vascular smooth muscle cell dynamics, cardiomyocyte hypertrophy, and fibrotic remodeling.[19] This investigation provides the first comprehensive analysis of LIMK1's involvement in ISO-mediated cardiomyocyte injury. Our data demonstrate that ISO stimulation markedly elevates LIMK1 expression in H9c2 cells, aligning with previous findings of upregulated LIMK1 in cardiac tissues from fibrotic rat models.[35] The study demonstrated that ISO exposure induced cardiomyocyte enlargement accompanied by reduced viability and proliferative capacity. Concurrently, we observed elevated secretion of cardiac injury biomarkers and upregulation of hypertrophic markers. Notably, *LIMK1* silencing

Published by Tehran University of Medical Sciences (http://ijaai.tums.ac.ir)

effectively attenuated these pathological alterations. Furthermore, our data revealed that *LIMK1* silencing substantially reduced ISO-induced expression of fibrosis-associated proteins and suppressed apoptotic cell death. These findings indicate that *LIMK1* inhibition mitigates ISO-triggered cardiomyocyte injury, hypertrophic responses, and fibrotic remodeling, highlighting its multifaceted involvement in myocardial pathological progression.

Studies have shown that the cardiovascular system is particularly susceptible to OS. Excessive ROS can directly damage cardiomyocytes, leading to tissue injury and functional impairment.[36–38] DCFH-DA fluorescence analysis demonstrated that ISO stimulation markedly elevated intracellular ROS levels in H9c2 cardiomyocytes, with concurrent intensification of 8-OHdG immunofluorescence signals, suggesting substantial oxidative DNA damage. Biochemical assays further revealed that ISO exposure significantly increased MDA content while suppressing SOD and GSH-Px activities, collectively indicating severe OS in cardiomyocytes. Research indicates that excessive ROS can damage cardiomyocytes through multiple pathways, including directly oxidizing proteins, lipids, and DNA, disrupting calcium homeostasis, activating pro-apoptotic signaling pathways, and inducing inflammation.[39] This study found that the increase in ROS induced by ISO was accompanied by hypertrophy, fibrosis, and apoptosis in cardiomyocytes, consistent with the multiple damage mechanisms of ROS. To further verify the key role of ROS in *LIMK1*-mediated cardiomyocyte protection, we performed intervention experiments by adding H_2O_2 (a ROS agonist) after *LIMK1* silencing. H_2O_2 co-treatment attenuated the cardioprotective effects of *LIMK1* knockdown against ISO-induced cellular damage, including hypertrophic, fibrotic, and apoptotic responses, substantiating ROS as a pivotal mediator in *LIMK1*-dependent cardiac injury.

Mitochondrial impairment represents a key pathological mechanism in ROS-induced cardiac injury.[40] Our experimental data demonstrated that ISO exposure triggered mitochondrial OS (MitoSOX) and depolarization (JC-1), confirming ISO-induced mitochondrial dysfunction. These findings align with previous reports of ROS-induced mitochondrial dysregulation in cardiomyocyte injury.[41] *LIMK1* knockdown effectively attenuated OS by reducing mitochondrial ROS accumulation and restoring membrane potential. Furthermore, both mitochondrial impairment and inflammatory activation are established contributors to HF pathogenesis.[42] In this study, ISO-induced inflammatory factor levels in H9c2 cardiomyocytes were significantly elevated, while *LIMK1* silencing significantly reduced the levels of inflammatory factors, suggesting that *LIMK1* silencing can ameliorate cardiomyocyte injury by inhibiting mitochondrial damage and inflammatory injury.

As a master transcriptional regulator, NF-κB coordinates fundamental biological processes spanning from immune-inflammatory cascades to proliferation and apoptosis control.[43,44] Under basal conditions, NF-κB remains sequestered in the cytoplasm through binding with its inhibitory subunit IκB. Upon cellular activation, IκB undergoes phosphorylation-dependent degradation, liberating NF-κB for nuclear translocation and subsequent transcriptional activation of target genes.[45] The NF-κB pathway critically contributes to HF pathogenesis by mediating cardiomyocyte hypertrophy, fibrosis, and apoptosis in response to OS, hypoxia, or inflammatory stimuli.[9] Concurrently, the NLRP3 inflammasome - a tripartite innate immune complex (NLRP3/ASC/caspase-1) - synergistically amplifies inflammatory responses during cardiac injury.[46] Previous studies have established that NLRP3 inflammasome activation occurs through multiple mechanisms, including NF-κB-dependent transcriptional upregulation of NLRP3 and pro-IL-1β, as well as ROS-mediated inflammasome assembly which triggers caspase-1 activation and subsequent maturation of IL-1β and IL-18.[47] This study pioneers the investigation of NF-κB/NLRP3 pathway activation in ISO-induced cardiomyocyte injury. ISO treatment enhanced the expression of NF-κB and NLRP3 and promoted activation of the NLRP3 inflammasome by activating the NF-κB/NLRP3 signaling pathway. Notably, *LIMK1* silencing effectively inhibited the expression of NF-κB and NLRP3 as well as the phosphorylation of NF-κB and IκB-α, while downregulating the expression of NLRP3 inflammasome–related proteins, indicating that *LIMK1* silencing attenuates inflammatory injury in cardiomyocytes by suppressing the NF-κB/NLRP3 signaling pathway. To further validate this mechanism, the NF-κB agonist dipro was added after *LIMK1* silencing for intervention experiments. The results showed that dipro treatment significantly reversed the inhibitory effects of *LIMK1* silencing on the production of inflammatory cytokines and concomitantly

upregulated the expression of NLRP3 inflammasome–related proteins, thereby further confirming the pivotal role of the NF-κB/NLRP3 signaling pathway in the *LIMK1*-mediated cardioprotective effects.

OS and inflammatory processes exhibit a complex bidirectional relationship, in which ROS function as key mediators of multiple pro-inflammatory signaling cascades, particularly the NF-κB pathway and NLRP3 inflammasome activation.[48–50] Mechanistically, ROS contribute to NLRP3 inflammasome stimulation through direct oxidative post-translational modifications of inflammasome components, as well as through indirect regulation of its assembly and subsequent activation. In this pioneering study, we comprehensively elucidate the mechanistic involvement of ROS-NF-κB/NLRP3 signaling in ISO-mediated cardiomyocyte damage. Our experimental data revealed that ISO stimulation potently enhanced the protein expression of both NF-κB pathway components and NLRP3 inflammasome elements. Importantly, pharmacological inhibition of ROS by NAC effectively normalized these aberrant protein expressions, while simultaneously mitigating multiple ISO-induced pathological manifestations including LDH leakage, cellular hypertrophy, fibrotic remodeling, apoptotic cell death, and inflammatory cytokine generation. The most compelling evidence emerged when co-administration of the NF-κB agonist dipro with NAC restored NF-κB/NLRP3 pathway activity and attenuated NAC's cardioprotection, definitively establishing ROS-dependent activation of NF-κB/NLRP3 signaling as a central regulatory mechanism in this cardiomyocyte injury model.

Although this study provides preliminary experimental evidence for the role of LIMK1 in ISO-induced myocardial injury, certain limitations exist that warrant further investigation in future research. Regarding validation of molecular biological mechanisms, the functional knockout experiments for LIMK1 in this study primarily relied on a single siRNA. While the results demonstrated significant silencing effects, parallel validation using multiple different siRNA sequences was not performed. In subsequent studies, we will employ multiple siRNAs targeting different LIMK1 sites and exogenous expression vector restoration experiments to more rigorously confirm the specificity of LIMK1-mediated effects. Second, the H9c2 cell line used in this study, derived from embryonic rat heart tissue, is widely employed in cardiomyopathy research. However, its skeletal muscle lineage prevents it from fully mimicking the contractile properties and complex electrophysiological characteristics of adult cardiomyocytes (e.g., selective expression of key cardiac ion channels). Future studies should incorporate primary cardiomyocytes or human induced pluripotent stem cell-derived cardiomyocytes (iPSC-CMs) for validation to enhance the biological validity of the conclusions. Furthermore, all current data originate from in vitro cellular models. While these models facilitate cellular and molecular-level analysis of LIMK1 mechanisms, they cannot fully reflect complex processes at the organismal level, such as cardiac structural remodeling, hemodynamic alterations, and multi-organ interplay. Therefore, subsequent studies should establish in vivo heart failure animal models that more closely mimic clinical disease progression. Through multilevel assessments, including cardiac function measurement, histology, and molecular biology, the role of LIMK1 in the development of heart failure and the efficacy of its intervention should be systematically validated. Additionally, 48-hour treatment with 10 μM ISO tends to induce acute adrenergic stress injury rather than fully mirroring the complex pathophysiology of chronic clinical heart failure. Furthermore, all biochemical and molecular expression analyses were conducted at a single time point. Given the highly dynamic evolution of HF-related signaling pathways (e.g., ROS-mediated NF-κB/NLRP3 axis), single-time-point observations may overlook critical stage-specific changes during disease progression. In summary, future research requires integrating dynamic multi-time-point observations, more physiologically relevant in vivo experimental models, and comprehensive validation using cardiomyocytes from diverse sources to further elucidate the pathological mechanisms of LIMK1 in heart failure and assess its potential as a clinical therapeutic target.

Our investigation reveals that *LIMK1* knockdown effectively diminishes ROS accumulation, blocks NF-κB/NLRP3 pathway stimulation, and consequently ameliorates OS, cellular enlargement, fibrotic changes, programmed cell death, and inflammatory responses in cardiomyocytes. This provides new ideas and a theoretical foundation for developing treatment strategies for HF. However, the current study was conducted only in the H9c2 cardiomyocyte cell line. Although in vitro experiments can effectively reveal

molecular mechanisms, certain limitations remain: on the one hand, the cell model cannot fully replicate the complex in vivo microenvironment and inter-organ interactions; on the other hand, the findings still need to be further validated in animal models and clinical samples for their physiological relevance. Future research will delve deeper into the *LIMK1*-regulated molecular network through in vivo experiments, aiming to provide a more reliable basis for targeting LIMK1 in HF treatment.

STATEMENT OF ETHICS

Not applicable.

FUNDING

Not applicable.

CONFLICT OF INTEREST

The authors declare no conflicts of interest.

ACKNOWLEDGMENTS

Not applicable.

DATA AVAILABILITY

The data that support the findings of this study are available from the corresponding author, upon reasonable request.

AI ASSISTANCE DISCLOSURE

Not applicable.

REFERENCES

1. Khan MS, Shahid I, Bennis A, Rakisheva A, Metra M, Butler J. Global epidemiology of heart failure. Nat Rev Cardiol. 2024;21(10):717-34.
2. Llego J, Bustillo KG. A Sequential Mixed Method Study on the Effectiveness of the Cardiac Enhancement Program Applied to Nursing Students. Nurs Sci Clin Practice. 2025;1(1):1-11.
3. Alnuwaysir RI, Hoes MF, van Veldhuisen DJ, van der Meer P, Grote Beverborg N. Iron deficiency in heart failure: mechanisms and pathophysiology. J Clin Med. 2021;11(1):125.
4. Roger VL. Epidemiology of heart failure: a contemporary perspective. Circ Res. 2021;128(10):1421-34.
5. Emmons-Bell S, Johnson C, Roth G. Prevalence, incidence and survival of heart failure: a systematic review. Heart. 2022;108(17):1351-60.
6. Lee H-H, Lee HA, Kim E-J, Kim HY, Kim HC, Ahn SH, et al. Metabolic dysfunction-associated steatotic liver disease and risk of cardiovascular disease. Gut. 2024;73(3):533-40.
7. Schwinger RH. Pathophysiology of heart failure. Cardiovascular Diagnosis Therapy. 2021;11(1):263.
8. Fonseka O, Gare SR, Chen X, Zhang J, Alatawi NH, Ross C, Liu W. Molecular Mechanisms Underlying Heart Failure and Their Therapeutic Potential. Cells. 2025;14(5).
9. Ghiasi M. Investigating the NF-κB signaling pathway in heart failure: Exploring potential therapeutic approaches. Heliyon. 2024;10(23).
10. Zhou J, Lin H, Lv T, Hao J, Zhang H, Sun S, et al. Inappropriate activation of TLR4/NF-κB is a cause of heart failure. Cardiovascular Innovations Applications. 2022;7(1):989.
11. Kowalczyk P, Sulejczak D, Kleczkowska P, Bukowska-Ośko I, Kucia M, Popiel M, et al. Mitochondrial oxidative stress—a causative factor and therapeutic target in many diseases. Int J Mol Sci. 2021;22(24):13384.
12. Xu S, Sun X, Wu J, Li K, Li X, Zhang Y, Gao X-j. TBBPA causes inflammation and cell death via the ROS/NF-κB pathway in the gastric mucosa. Ecotoxicol Environmental Safety. 2023;262:115320.
13. Blevins HM, Xu Y, Biby S, Zhang S. The NLRP3 inflammasome pathway: a review of mechanisms and inhibitors for the treatment of inflammatory diseases. Front Aging Neuroscience. 2022;14:879021.
14. Ashrafizadeh M. Cell death mechanisms in human cancers: molecular pathways, therapy resistance and therapeutic perspective. J Cancer Biomol Therapeutics. 2024;1(1):17-40.
15. Moradi A, Aslani MR, Mirshekari Jahangiri H, Naderi N, Aboutaleb N. Protective effects of 4-methylumbelliferone on myocardial ischemia/reperfusion injury in rats through inhibition of oxidative stress and downregulation of TLR4/NF-κB/NLRP3 signaling pathway. Naunyn Schmiedebergs Arch Pharmacol. 2024;397(7):5015-27.
16. Lateef OM, Foote C, Power G, Manrique-Acevedo C, Padilla J, Martinez-Lemus LA. LIM kinases in cardiovascular health and disease. Front Physiol. 2024;15:1506356.

17. Villalonga E, Mosrin C, Normand T, Girardin C, Serrano A, Žunar B, et al. LIM kinases, LIMK1 and LIMK2, are crucial node actors of the cell fate: molecular to pathological features. Cells. 2023;12(5):805.
18. Ribba A-S, Fraboulet S, Sadoul K, Lafanechère L. The role of LIM kinases during development: a lens to get a glimpse of their implication in pathologies. Cells. 2022;11(3):403.
19. Lateef OM, Foote C, Power G, Manrique-Acevedo C, Padilla J, Martinez-Lemus LA. LIM kinases in cardiovascular health and disease. Frontiers in Physiology. 2024;15:1506356.
20. Chen Y, Song D, Gao J, Zhang X, Chen X. Circ-Zfp644 acts as a pro-hypertrophic mediator in an Ang-II induced in vitro myocardial hypertrophy model. Cell Biol Int. 2021;45(6):1260-8.
21. Gong C, Chang L, Huang R, Sun X, Liu Y, Wu S, et al. LIM kinase 2 activates cardiac fibroblasts and exacerbates postinfarction left ventricular remodeling via crosstalk between the canonical and non-canonical Wnt pathways. Pharmacol Res. 2024;208:107347.
22. Su Q, Zhang P, Yu D, Wu Z, Li D, Shen F, et al. Upregulation of miR-93 and inhibition of LIMK1 improve ventricular remodeling and alleviate cardiac dysfunction in rats with chronic heart failure by inhibiting RhoA/ROCK signaling pathway activation. Aging (Albany NY). 2019;11(18):7570-86.
23. Hu L, Wang Z, Li H, Wei J, Tang F, Wang Q, et al. Icariin inhibits isoproterenol-induced cardiomyocyte hypertropic injury through activating autophagy via the AMPK/mTOR signaling pathway. Biochem Biophysical Res Commun. 2022;593:65-72.
24. Zhao R, Zhao D, Zhu X, Li F, Xiong P, Li S, Liu J. The influence of miR-3149 on the malignancy progression of gastric cancer by negatively regulating CEACAM5. J Cancer Biomol Therapeutics. 2024;1(1):1-10.
25. He D, Yan L. MiR-29b-3p aggravates cardiac hypoxia/reoxygenation injury via targeting PTX3. Cytotechnology. 2021;73(1):91-100.
26. Liu P, Vairaperumal T, Lee Y, Tsai T. Activation of fibroblast growth factor 21 by Canagliflozin reduces high-fat diet associated obesity-related cardiac injury: a translational study from bench to bedside. Europ Heart J. 2024;45(Supplement_1):ehae666. 2897.
27. Du L, Lu H, Wang Z, Liu C, Xiao Y, Guo Z, Li Y. Therapeutic potential of ginsenoside Rb1-PLGA nanoparticles for heart failure treatment via the ROS/PPARα/PGC1α pathway. Molecules. 2023;28(24):8118.
28. Alam P, Maliken BD, Jones SM, Ivey MJ, Wu Z, Wang Y, Kanisicak O. Cardiac remodeling and repair: recent approaches, advancements, and future perspective. Int J Mol Sci. 2021;22(23):13104.
29. Gunata M, Parlakpinar H. A review of myocardial ischaemia/reperfusion injury: pathophysiology, experimental models, biomarkers, genetics and pharmacological treatment. Cell Biochem function. 2021;39(2):190-217.
30. Niu J, Li Y, Song X, Liu Y, Li Y, Li Y. Cardioprotective effect of echinatin against ischemia/reperfusion injury: involvement of Hippo/Yes-associated protein signaling. Front Pharmacol. 2021;11:593225.
31. Guo M, Xu J, Long X, Liu W, Aris AZ, Yang D, et al. Myocardial fibrosis induced by nonylphenol and its regulatory effect on the TGF-β1/LIMK1 signaling pathway. Ecotoxicol Environ Saf. 2024;272:116110.
32. Cen Y, Xiong Y, Qin R, Tao H, Yang Q, Pan X. Anti-malarial artesunate ameliorates atherosclerosis by modulating arterial inflammatory responses via inhibiting the NF-κB–NLRP3 inflammasome pathway. Front Pharmacol. 2023;14:1123700.
33. Huang Y, Xu W, Zhou R. NLRP3 inflammasome activation and cell death. Cell Mol Immunol. 2021;18(9):2114-27.
34. Noh J-M, Choi S-C, Song M-H, Kim KS, Jun S, Park JH, et al. The Activation of the LIMK/Cofilin Signaling Pathway via Extracellular Matrix–Integrin Interactions Is Critical for the Generation of Mature and Vascularized Cardiac Organoids. Cells. 2023;12(16):2029.
35. Guo M, Xu J, Long X, Liu W, Aris AZ, Yang D, et al. Myocardial fibrosis induced by nonylphenol and its regulatory effect on the TGF-β1/LIMK1 signaling pathway. Ecotoxicol Environmental Safety. 2024;272:116110.
36. Xiang M, Lu Y, Xin L, Gao J, Shang C, Jiang Z, et al. Role of oxidative stress in reperfusion following myocardial ischemia and its treatments. Oxidative Med Cell longevity. 2021;2021(1):6614009.
37. Yan Q, Liu S, Sun Y, Chen C, Yang S, Lin M, et al. Targeting oxidative stress as a preventive and therapeutic approach for cardiovascular disease. J Trans Med. 2023;21(1):519.
38. Akhigbe R, Ajayi A. The impact of reactive oxygen species in the development of cardiometabolic disorders: a review. Lipids Health Dis. 2021;20(1):23.
39. Zadorozny L, Du J, Supanekar N, Annamalai K, Yu Q, Wang M. Caveolin and oxidative stress in cardiac pathology. Front Physiol. 2025;16:1550647.

40. Yi C, Song M, Sun L, Si L, Yu D, Li B, et al. Asiatic acid alleviates myocardial ischemia-reperfusion injury by inhibiting the ROS-mediated mitochondria-dependent apoptosis pathway. Oxidative Med Cell Longevity. 2022;2022(1):3267450.
41. Xu Z, Li J, Su B, Gao H, Ren M, Lin Y, Shen H. A role of ROS-dependent defects in mitochondrial dynamic and autophagy in carbon black nanoparticle-mediated myocardial cell damage. Free Radical Biol Med. 2024;220:249-61.
42. Hinton Jr A, Claypool SM, Neikirk K, Senoo N, Wanjalla CN, Kirabo A, Williams CR. Mitochondrial structure and function in human heart failure. Circul Res. 2024;135(2):372-96.
43. Green DR. The death receptor pathway of apoptosis. Cold Spring Harbor Perspectives in Biol. 2022;14(2):a041053.
44. Zhang T, Ma C, Zhang Z, Zhang H, Hu H. NF-κB signaling in inflammation and cancer. Med Comm. 2021;2(4):618-53.
45. Adlimoghaddam A, Albensi BC. The nuclear factor kappa B (NF-κB) signaling pathway is involved in ammonia-induced mitochondrial dysfunction. Mitochondrion. 2021;57:63-75.
46. Castillo RL, Farías J, Sandoval C, González-Candia A, Figueroa E, Quezada M, et al. Role of NLRP3 Inflammasome in Heart Failure Patients Undergoing Cardiac Surgery as a Potential Determinant of Postoperative Atrial Fibrillation and Remodeling: Is SGLT2 Cotransporter Inhibition an Alternative for Cardioprotection? Antioxidants. 2024;13(11):1388.
47. Ramachandran R, Manan A, Kim J, Choi S. NLRP3 inflammasome: a key player in the pathogenesis of life-style disorders. Exp Mol Med. 2024;56(7):1488-500.
48. Liu Wb, Wang Ss, Zhang X, Ke Zz, Wen Xy, Zhao J, et al. Enhanced Cardiomyocyte NLRP3 Inflammasome-Mediated Pyroptosis Promotes d-Galactose–Induced Cardiac Aging. J A Heart Association. 2024;13(14):e032904.
49. Sul O-J, Ra SW. Quercetin prevents LPS-induced oxidative stress and inflammation by modulating NOX2/ROS/NF-kB in lung epithelial cells. Molecules. 2021;26(22):6949.
50. Donia T, Khamis A. Management of oxidative stress and inflammation in cardiovascular diseases: mechanisms and challenges. Environ Sci Pollut Res Int. 2021;28(26):34121-53.